International Journal of Multiphase Flow 36 (2010) 51–59

Contents lists available at ScienceDirect

International Journal of Multiphase Flow

journal homepage: www.elsevier.com/locate/ijmulflow

Quadrature method of moments for modeling multi-component spray vaporization

Claire Laurent *, Gerard Lavergne, Philippe Villedieu

ONERA/DMAE, 2 av. Edouard Belin BP 74025, 31055 Toulouse, France

ARTICLE INFO

Article history:
Received 1 October 2008
Received in revised form 27 August 2009
Accepted 28 August 2009
Available online 3 September 2009

Keywords:
Droplet
Vaporization
Multi-component mixture
Quadrature method of moments

ABSTRACT

This article puts forward the quadrature method of moments (QMoM) for modeling droplet composition during the spray vaporization process. This method is implemented for solving the *Continuous Thermodynamic Model* (CTM) of multi-component droplet vaporization, an advantageous alternative to the classical *Discrete Component Model* (DCM) when the droplet is formed of a great number of components. The CTM approach consists in modeling the droplet's composition using a probability density function (PDF). This method was first tried out for vaporizing droplets by Hallett, who assumed a Gamma-function for the PDF. However, Harstadt et al. underlined some problems in the case of vapor condensation on the droplet surface, since the Gamma-PDF model presumes the PDF's mathematical form. The QMoM which does not require this hypothesis is studied in this article, according to Lage's research dealing with QMoM application to phase equilibria. The numerical features of QMoM are investigated in detail, and then the method is implemented for the difficult test case of vapor condensation. The results are analyzed to illustrate the application of QMoM to multi-component droplet vaporization modeling and to provide a better understanding of the QMoM main advantages and limitations.

1. Introduction

Droplet vaporization is a phenomenon that has been studied for years, both from experimental and theoretical points of view. An extensive review of studies dealing with this subject is given by Sirignano in his reference book (Sirignano, 1999) and covers phenomena from the behavior of a single droplet to the interactions between droplets in a spray. The modeling of droplet physics is actually becoming a real issue in light of the emergence of many applications requiring droplet spray technologies. From propulsion applications in the aerospace or automotive industries to the nuclear and pharmaceutical industries, droplet spray control is a challenge faced by numerous strategic technologies. The optimization of designs entails the substantial development of physical modeling. In particular in the field of engine technologies, continuous performance improvements require the phenomenon of multi-component droplet vaporization to be considered, since pollutant emissions and new fuel efficiency depend directly on droplet composition.

The modeling of multi-component droplet vaporization was first studied with the aim of rigorously describing the concentration evolution of each droplet component: this is the *Discrete Component Model* (DCM) (Sirignano, 1999). However, the implementation of such a model in CFD codes is not ideal, due to its excessive computational cost, induced both by the use of a multi-component model for the vaporization process and by the implementation of a transport equation for each vapor component in the gas phase. The *Continuous Thermodynamic Model* (CTM), first developed in the chemical field by Cotterman et al. (1985), is a worthwhile approach in which droplet composition is modeled by a probability density function (PDF). In their first study, the authors assumed the PDF's mathematical form to solve the vapor–liquid equilibrium using a Γ function. This method was then extended to multi-component droplet vaporization by Hallett (2000) and was also implemented by Harstadt et al. who pointed out the weakness of the method in the case of vapor condensation (Harstadt et al., 2003). In this case, the assumption about the PDF shape is actually no longer verified and the implementation of the Γ-CTM approach in CFD codes is therefore not straightforward. Indeed, even though this phenomenon is not preponderant for combustion applications, it can occur due to local inhomogeneities and lead to computation failure. New methods in which the PDF is not presumed were then investigated, such as Orthogonal Collocation (OC) which was developed recently by Arias-Zugasti and Rosner (2003). The quadrature method of moments (QMoM) is based on the same motivation and draws its interest from some outstanding properties provided by its mathematical background. The QMoM has already been applied successfully for modeling multi-component phenomena, such as phase equilibria (Lage, 2007), and in other application fields too, such as aerosol dynamics (McGraw, 1997), population balance equations (Marchisio and Fox, 2005) and particle-laden flows (Desjardins et al., 2008). A preliminary study has shown that QMoM is also relevant for modeling

* Corresponding author. Tel.: +33 562252826; fax: +33 562252583.
E-mail address: claire.laurent@onera.fr (C. Laurent).

0301-9322/$ - see front matter © 2009 Elsevier Ltd. All rights reserved.
doi:10.1016/j.ijmultiphaseflow.2009.08.005

multi-component droplet vaporization (Laurent et al., 2009), and consequently numerical properties of QMoM are investigated in detail in this article in order to demonstrate its advantages for its implementation in CFD codes.

In the first part of this article, the method is presented in detail, both the technical approach (i.e. the model and the algorithm) and the mathematical concepts which are at the root of the method. The originality of the paper comes from the analysis of the so-called mathematical *Moment Problem* which corresponds to the application of the QMoM to the droplet vaporization phenomenon. In particular, the theoretical foundations of *Moment Problems* enable some relevant properties for QMoM robustness to be put forward. Then, in the second part of the article, the QMoM is tested when vapor condenses at the droplet surface. The results are analyzed to study the convergence and the efficiency of the QMoM and subsequently to point out the model's qualities and defects.

2. Application of QMoM for modeling multi-component droplet vaporization

In this first part, the application of QMoM to the multi-component droplet vaporization phenomenon is explained and some key points are highlighted to put forward the method's relevant properties.

2.1. Continuous modeling of the droplet composition

In the studied models, the droplet is assumed to have a uniform composition which gradually shifts during the vaporization process, due to the volatility difference between components. In the *Discrete Component Model* (DCM), the mole fraction x_l^i of each component i is computed. The *Continuous Thermodynamic* model allows to reduce the computational cost by modeling the droplet's composition with a probability density function (PDF). This PDF f_l is defined by $x_l^i = f_l(I)\Delta I$. The distribution parameter is selected in order to best characterize a component considering its physical behavior for vaporization process. The normal boiling point T_{nb} is a relevant feature for vaporization phenomenon since, contrary to the molar mass which is commonly used (Hallett, 2000; Harstadt et al., 2003), it is a direct parameter for the heat of vaporization and the saturation vapor pressure relationships (see Eqs. (5) and (23)). This parameter is then chosen for the *Continuous Thermodynamic Model* (CTM) and the QMoM implementation.

The representation of the droplet composition in the QMoM approach can be interpreted as a *Discrete Component Model* with N pseudo-components (denoted by the subscript k) instead of $\mathcal{N}$ real components (denoted by the subscript i). Indeed, the PDF is the sum of $N\delta$ functions, determined by the mole fraction $\hat{x}_l^k$ and the normal boiling point $\hat{I}_l^k$ of the N pseudo-components. These quantities are then based on N so-called environments, where an environment corresponds to a single δ-peak. Therefore, the QMoM approach presumes a multi-environment PDF:

$$f_{l,N}(I) = \sum_{k=1}^{N} \hat{x}_l^k \delta_{\hat{I}_l^k}(I) \tag{1}$$

The number of pseudo-components is very small compared with the number of real components ($N \ll \mathcal{N}$) and the normal boiling point T_{nb} of each pseudo-component is changing during the vaporization process in order to best fit the real droplet composition PDF. This explains the name of "pseudo-component" used to clarify QMoM description (Lage, 2007). Another way for mathematically modeling the droplet's composition is given by the PDF's moments. The α order moment of the droplet's composition is defined from the PDF by

$$m_l^\alpha = \int_0^{+\infty} f_l(I) I^\alpha dI \tag{2}$$

In the QMoM approach, the integration is simply reduced to a discrete sum:

$$m_l^\alpha = \sum_{k=1}^{N} \hat{x}_l^k \left(\hat{I}_l^k\right)^\alpha \tag{3}$$

The set of equations satisfied by these moments is obtained from the PDF moment equations modeling droplet vaporization process (see Section 2.3). The derivation of this equation requires a specific modeling of physical properties in the framework of *Continuous Thermodynamics*. This is detailed in the next section.

2.2. Physical properties for the continuous thermodynamic modeling

In the *Continuous Thermodynamic* approach, the physical properties have to be interpolated as functions of $I = T_{nb}$. This is the first hypothesis, denoted **Hypothesis 1** in this paper, assumed by CTM models. In the case of complex mixtures, the components are classified into homogeneous groups such as paraffins, iso-paraffins, alcohols or mono-aromatics in order to ensure a satisfying modeling of physical properties in the framework of *Continuous Thermodynamics*. This first assumption implies to reach a compromise between a reliable description of the droplet's composition and the multiplicity of groups. The choice of the distribution parameter affects also this compromise, and the normal boiling point $I = T_{nb}$ is then a relevant option since, in this case, only one component group can be suitable for modeling fuels such as kerosene.

The physical properties of pseudo-components are therefore relative to their boiling point. The coefficients of laws corresponding to various physical properties are interpolated as function of the distribution parameter I (see Appendix A). The procedure is explained for the normal latent heat of vaporization l_{vb} which is used to compute the saturation vapor pressure P_{sat} (see Eq. (23)) and the latent heat of vaporization l_v (see Eq. (4)). For real components, the expression of l_v commonly used in literature is (Reid et al., 1977)

$$l_v^i = l_{vb}^i \left(\frac{T_c^i - T_s}{T_c^i - T_{nb}^i}\right)^{0.38} \tag{4}$$

In this formula, l_{vb} and T_c (the critical temperature) are interpolated as functions of I to obtain the relationship for l_v in the framework of *Continuous Thermodynamics*:

$$l_v(I) = l_{vb}(I) \left(\frac{T_c(I) - T_s}{T_c(I) - I}\right)^{0.38} \tag{5}$$

The interpolation law for l_{vb} has been established from a study on real components considering l_{vb} variations versus T_{nb}. A quasi-linear evolution is obtained (see Fig. 1) and then, l_{vb} is computed using

$$l_{vb}(I) = A_0 + A_1 I \tag{6}$$

Concerning the other physical properties, the coefficients of the corresponding laws have been mainly linearly interpolated, except for the liquid molar volume density and the liquid viscosity relationships which use second order polynomials (see Appendix A).

Concerning the modeling of heterogeneous compositions, several groups of components can be used to improve the accuracy of the *Continuous Thermodynamic* approach. In the following sections, the models are only detailed for one component group, since the multi-PDF model is merely an extension which uses classical *Discrete Component Model* applied to groups instead of components.

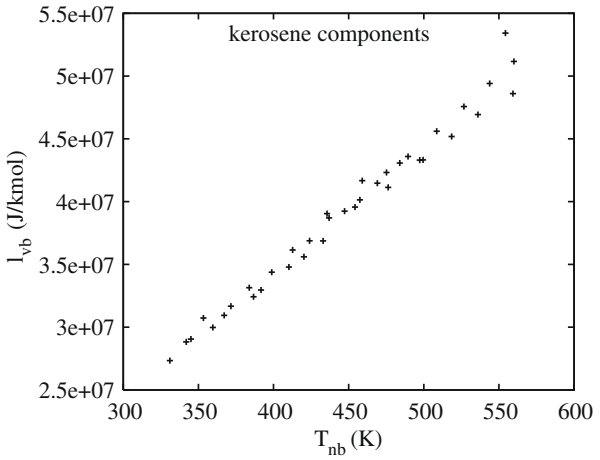

Fig. 1. Normal latent heat of vaporization l_{vb} for each component of the kerosene.

2.3. PDF moment equations for modeling droplet composition evolution

When the composition is assumed to be uniform in the droplet, the mass conservation equation for each component i is

$$\frac{dx_l^i}{dt} = \frac{3}{4\pi R^3 c_l}\left(\dot{n}^{tot}x_l^i - \dot{n}^i\right) \tag{7}$$

This equation gives the evolution of the mole fraction x_l^i of the real component i in the droplet whose radius is R. This relationship is written using the molar system since it is more convenient for *Continuous Thermodynamic* methods (mole fractions are commonly used for physical properties of mixtures). Then, c_l represents the molar volume density of the droplet, $\dot{n}^i$ the molar vapor flow rate of the component i and $\dot{n}^{tot}$ the total vapor flow rate.

Classical droplet vaporization models assume quasi-steadiness and spherical symmetry for the surrounding gas phase (r is the radial coordinate). The vapor flow rate $\dot{n}^i$ of each real component i is modeled by the sum of a convection and a diffusion term. The diffusion term is modeled using a simplified *Fick's law* with a diagonal diffusion matrix whose values are the diffusion coefficients D_g^i:

$$\dot{n}^i = \dot{n}^{tot}x_g^i - 4\pi r^2 c_g D_g^i \frac{dx_g^i}{dr} \tag{8}$$

Then, the *Sherwood* number Sh_g^i, defined by

$$Sh_g^i = \frac{2R}{x_{g,\infty}^i - x_{g,S}^i}\left(\frac{dx_g^i}{dr}\right)_s \tag{9}$$

is introduced and Eq. (8) is applied at the droplet surface (i.e. $r = R$). This gives the vapor flow rate $\dot{n}^i$ according to the mole fractions $x_{g,s}^i$ and $x_{g,\infty}^i$ which correspond respectively to the mole fractions of the component i at the droplet surface and at the droplet boundary layer limit (infinity if the droplet is unmoving):

$$\dot{n}^i = \dot{n}^{tot}x_{g,s}^i - 2\pi R c_g D_g^i Sh_g^i\left(x_{g,\infty}^i - x_{g,s}^i\right) \tag{10}$$

Therefore, Eq. (7) modeling droplet composition evolution becomes:

$$\frac{dx_l^i}{dt} = \frac{3}{4\pi R^3 c_l}\left(\dot{n}^{tot}x_l^i - \dot{n}^{tot}x_{g,s}^i + 2\pi R c_g D_g^i Sh_g^i\left(x_{g,\infty}^i - x_{g,s}^i\right)\right) \tag{11}$$

In order to convert this equation in the *Continuous Thermodynamic* framework, the diffusion coefficients D_g^i and the *Sherwood* numbers Sh_g^i are assumed to be the same for all components. Indeed, this hypothesis (called **Hypothesis 2** in the paper) is commonly done by *Continuous Thermodynamic Models* to perform the integration of the continuous form of Eq. (11) and then, to obtain PDF moment equations. This assumption may seem quite strong since it supposes the same diffusion behavior for all vapor components. The practical experience shows some consequences in certain cases when the vapor composition is rather different from the droplet composition. However, even for these unfavourable cases, the results remain quite satisfactory (see Section 3).

The *Spalding* number B_M is commonly introduced in droplet vaporization models. Its definition is

$$B_M = \frac{x_{g,s}^{tot} - x_{g,\infty}^{tot}}{1 - x_{g,s}^{tot}} \tag{12}$$

The total vapor mole fraction $x_{g,\infty}^{tot}$ is known and $x_{g,s}^{tot}$ is obtained from the phase equilibrium at the droplet interface. This point is detailed below in Section 2.5. Then, the sum of Eq. (10) for all components i using **Hypothesis 2** assumption and B_M definition yields

$$\dot{n}^{tot} = 2\pi R c_g D_g Sh_g B_M \tag{13}$$

This equation is used in Eq. (11) to replace $Sh_g D_g$ and, for $\dot{n}^{tot} \neq 0$ (i.e., $B_M \neq 0$), this gives:

$$\frac{dx_l^i}{dt} = \frac{3\dot{n}^{tot}}{4\pi R^3 c_l}\left(x_l^i - \frac{x_{g,s}^i(1+B_M) - x_{g,\infty}^i}{B_M}\right) \tag{14}$$

and, for $\dot{n}^{tot} = 0$,

$$\frac{dx_l^i}{dt} = \frac{3c_g D_g Sh_g}{2R^2 c_l}\left(x_{g,\infty}^i - x_{g,s}^i\right) \tag{15}$$

This modeling is then transposed into the CTM framework and the integration of the continuous form of Eqs. (14) and (15) gives the moment evolution equations. In the case of $\dot{n}^{tot} \neq 0$ (i.e., $B_M \neq 0$), the PDF moment equations are:

$$\frac{dm_l^\alpha}{dt} = \frac{3\dot{n}^{tot}}{4\pi R^3 c_l}\left(m_l^\alpha - \frac{m_{g,s}^\alpha(1+B_M) - m_{g,\infty}^\alpha}{B_M}\right) \tag{16}$$

and, in the case of $\dot{n}^{tot} = 0$, this is

$$\frac{dm_l^\alpha}{dt} = \frac{3c_g D_g Sh_g}{2R^2 c_l}\left(m_{g,\infty}^\alpha - m_{g,s}^\alpha\right) \tag{17}$$

These equations constitute the *Moment Problem* which has to be solved numerically. All parameters defined in the right-hand side of these equations are known, except the total vapor flow rate $\dot{n}^{tot}$ (see the detail of calculation in the next section) and the PDF moments at the droplet surface $m_{g,s}^\alpha$ (see Section 2.5).

2.4. Vapor flow rate calculation

The total vapor flow rate $\dot{n}^{tot}$ is calculated following the classical modeling of the droplet vaporization phenomenon (Sirignano, 1999). The integration of Eq. (8) on the boundary layer of the droplet, between the droplet radius R and the limit of the boundary layer R_f, gives

$$x_{g,s}^{tot} = 1 + \left(x_{g,\infty}^{tot} - 1\right)exp\left(-\frac{\dot{n}^{tot}}{4\pi c_g D_g}\left(\frac{1}{R} - \frac{1}{R_f}\right)\right) \tag{18}$$

Using B_M definition (see Eq. (12)), this leads to the well-known equation (Sirignano, 1999):

$$\dot{n}^{tot} = 2\pi R c_g D_g Sh_g^* ln(1 + B_M) \tag{19}$$

where Sh_g^* is the *modified Sherwood* number defined by:

$$Sh_g^* = \frac{2R_f}{R_f - R} \tag{20}$$

For an unmoving droplet, $Sh_g^* = 2$ since $R_f \to \infty$ and in general, Sh_g^* is given by correlations depending on the *Reynolds* number, the *Schmidt* number and the *Spalding* number (Sirignano, 1999).

2.5. Vapor–liquid equilibrium at the droplet surface

The vapor–liquid equilibrium at the droplet interface enables to compute the moments of the vapor composition at the droplet surface $\{m_{g,s}^\alpha\}_0^{2N-1}$ from the moments of the droplet composition $\{m_l^\alpha\}_0^{2N-1}$. For ideal mixtures, the phase equilibrium at the droplet interface finds expression in the well-known *Raoult's law*,

$$x_{g,s}^i P_\infty = x_l^i P_{sat}^i(T_s) \tag{21}$$

where $P_{sat}(T_s)$ refers to the saturation vapor pressure expressed at T_s, the temperature at the droplet surface. The continuous form of Eq. (21) is

$$f_{g,s}(I) P_\infty = f_l(I) P_{sat}(I, T_s) \tag{22}$$

and P_{sat} is given, for instance, by the *Clausius-Clapeyron* equation:

$$P_{sat}(I, T_s) = P_\infty exp\left(\frac{l_{vb}(I)}{\mathscr{R}}\left(\frac{1}{I} - \frac{1}{T_s}\right)\right) \tag{23}$$

The integration of Eq. (22) gives the expression which joins the moments $\{m_{g,s}^\alpha\}_0^{2N-1}$ to the moments $\{m_l^\alpha\}_0^{2N-1}$. The non-polynomial function $I \to P_{sat}(I)$ (see Eq. (23)) reveals that the integration of the vapor–liquid equilibrium equation can be a difficult point depending on the PDF expression. For the Γ-CTM approach, this was solved by Cotterman et al. (1985) and then resumed by Hallett for vaporizing droplet modeling (Hallett, 2000). Concerning the method proposed in this paper, the difficulty is taken back to find the mole fraction $\hat{x}_l^k$ and the normal boiling point $\widehat{I}_l^k$ of each pseudo-component k. Indeed, the integration of the continuous form of the *Raoult's law* (see Eq. (22)) using the QMoM PDF $f_{l,N}$ (see Eq. (1)) gives:

$$m_{g,s}^\alpha = \sum_{k=1}^{N} \hat{x}_l^k \frac{P_{sat}\left(\widehat{I}_l^k, T_s\right)}{P_\infty} \left(\widehat{I}_l^k\right)^\alpha \tag{24}$$

The key point is now the computation of the $\{\widehat{I}_l^k\}_1^N$ and the $\{\hat{x}_l^k\}_1^N$ from the set of moments $\{m_l^\alpha\}_0^{2N-1}$ numerically computed from Eq. (16). This problem is commonly called a *Moment Problem* in mathematics.

2.6. The Moment Problem

The *Moment Problem* studied in this paper consists in searching the N nodes $\{\widehat{I}_l^k\}_1^N$ and the N weights $\{\hat{x}_l^k\}_1^N$ of a *Gauss quadrature* whose formulation for this application is

$$\int F(I) f_{l,N}(I) dI = \sum_{k=1}^{N} \hat{x}_l^k F\left(\widehat{I}_l^k\right) + \mathscr{R}(F) \tag{25}$$

$$\mathscr{R}(\mathbb{P}^{2N-1}) = 0 \tag{26}$$

Indeed, when $F(I) = I^\alpha$ in this expression, the *Gauss quadrature* gives an exact solution for the moments up to the $2N-1$ order. This quadrature rule is optimal since N nodes are necessary and sufficient to obtain the $2N$ first moments.

2.7. Proof of the existence of a solution to the studied Moment Problem

At each time step, moments are computed by discretizing Eq. (16). The numerical expression at $t + \Delta t$ is then

$$m_l^\alpha(t+\Delta t) = \left(1 + \frac{3\dot{n}^{tot}}{4\pi R^3 c_l}\Delta t\right) m_l^\alpha(t) - \frac{3\Delta t}{4\pi R^3 c_l} \times \frac{\dot{n}^{tot}(1+B_M)}{B_M} m_{g,s}^\alpha(t) + \frac{3\Delta t}{4\pi R^3 c_l}\frac{\dot{n}^{tot}}{B_M} m_{g,\infty}^\alpha(t) \tag{27}$$

The PDF $f_{l,N}$ associated to the moments $\{m_l^\alpha\}_0^{2N-1}$ is supposed to exist at time t. Then, after using Eq. (22), Eq. (27) is equivalent to

$$m_l^\alpha(t+\Delta t) = \int I^\alpha (A f_{l,N} + B f_{g,\infty,N} s) dI \tag{28}$$

with

$$A(I,t) = \left(1 + \frac{3\dot{n}^{tot}(t)}{4\pi(R(t))^3 c_l(t)}\Delta t\right) - \frac{3\Delta t}{4\pi(R(t))^3 c_l(t)} \times \frac{\dot{n}^{tot}(t)(1+B_M(t))}{B_M(t)} \frac{P_{sat}(I,t)}{P_\infty} \tag{29}$$

and

$$B(t) = \frac{3\Delta t}{4\pi(R(t))^3 c_l(t)} \frac{\dot{n}^{tot}(t)}{B_M(t)} \tag{30}$$

The issue discussed in this section is to know which constraint should be satisfied by the time step to ensure the existence at time $t + \Delta t$ of a N-point PDF having exactly the $2N$ first moments $\{m_l^\alpha(t+\Delta t)\}_0^{2N-1}$. According Shohat and Curto who studied mathematically *Moment Problems*, the positivity of *Hankel* matrices H_{N-1} and H_{N-1}^* obtained from moments $\{m_l^\alpha\}_0^{2N-1}$ is a necessary and sufficient condition for the existence of a N-point PDF on $]0;+\infty[$ (Shohat and Tamarkin, 1943; Curto and Fialkow, 1991). These *Hankel* matrices are defined by:

$$H_{N-1} = \begin{pmatrix} m_l^0 & m_l^1 & \cdots & m_l^{N-1} \\ m_l^1 & m_l^2 & \cdots & m_l^N \\ \vdots & \vdots & \ddots & \vdots \\ m_l^{N-1} & m_l^N & \cdots & m_l^{2N-2} \end{pmatrix} \tag{31}$$

and

$$H_{N-1}^* = \begin{pmatrix} m_l^1 & m_l^2 & \cdots & m_l^N \\ m_l^2 & m_l^3 & \cdots & m_l^{N+1} \\ \vdots & \vdots & \ddots & \vdots \\ m_l^N & m_l^{N+1} & \cdots & m_l^{2N-1} \end{pmatrix} \tag{32}$$

Then, in order to prove the positivity of *Hankel* matrices at time $t + \Delta t$, the function $I \to A(I,t) f_l^j(I,t) + B(t) f_{g,\infty}^j(I,t)$ is studied. The function B is always positive, and a lower bound is obtained for $I \to A(I,t)$:

$$A(I,t) \geqslant \left(1 + \frac{3\dot{n}^{tot}}{4\pi R^3 c_l}\Delta t\right) - \frac{3\Delta t}{4\pi R^3 c_l}\frac{\dot{n}^{tot}(1+B_M)}{B_M} max_k\left(\frac{P_{sat}(\widehat{I}_l^k)}{P_\infty}\right) \tag{33}$$

Indeed, the following inequality Eq. (34) has been introduced in Eq. (29) for the saturation vapor pressure term:

$$min_k\left(\frac{P_{sat}(\widehat{I}_l^k)}{P_\infty}\right) \leqslant \frac{P_{sat}(I)}{P_\infty} \leqslant max_k\left(\frac{P_{sat}(\widehat{I}_l^k)}{P_\infty}\right) \tag{34}$$

Finally, different cases have been distinguished according to the sign of each term of Eq. (33), and a sufficient condition on Δt has been found to ensure the positivity of the lower bound of A. After some calculations, this leads to

$$\Delta t < \frac{\left|\frac{\frac{4}{3}\pi R^3 c_l}{\dot{n}^{tot}}\right|}{\left|-1 + \frac{(1+B_M)}{B_M} max_k\left(\frac{P_{sat}(\widehat{I}_l^k)}{P_\infty}\right)\right|} \tag{35}$$

In the case of $\dot{n}^{tot} = 0$, this inequality must be replaced by

$$\Delta t < \frac{\frac{4}{3}\pi R^3 c_l}{\left|2\pi R c_g D_g Sh_g max_k\left(\frac{P_{sat}(\widehat{I}_l^k)}{P_\infty}\right)\right|} \tag{36}$$

This criterion can be easily compared to the characteristic vaporization time of a mono-component droplet, since the lifetime given by the D^2-law in this case is

$$\tau = \left|\frac{3}{2}\frac{\frac{4}{3}\pi c_l R^3}{\dot{n}^{tot}}\right| \tag{37}$$

Consequently, there exists Δt such that the function $I \to A(I,t)f_l^j(I,t) + B(t)f_{g,\infty}^j(I,t)$ is positive. This entails the positivity of *Hankel* matrices at $t + \Delta t$ and subsequently, according to the *Moment Problem* theory, this proves the existence of a N-point PDF at $t + \Delta t$ having exactly the $2N$ first moments $\{m_l^\alpha(t + \Delta t)\}_0^{2N-1}$.

The existence of a solution to the studied *Moment Problem* is thus theoretically proved under an explicit condition about the time step. This result is one of the main points of interest of QMoM since it demonstrates its robustness and therefore its potential for implementation in CFD codes.

2.8. QMoM algorithm for computing nodes and weights

The mathematical background of the method is used to built the QMoM algorithm which finds the nodes $\{\widehat{I}_l^k\}_1^N$ and the weights $\{\hat{x}_l^k\}_1^N$ of the *Gauss quadrature* (see Eq. (25)). According to the fundamental theorem of *Gauss quadrature* (Gautschi, 2004; Press and Teukolsky, 1990), the nodes are the roots of the monic orthogonal polynomial π_N relative to the inner product defined by

$$\langle p, q\rangle = \int_0^{+\infty} p(I)q(I)f_{l,N}(I)dI \tag{38}$$

Then, as any orthogonal polynomial sequence, the $\{\pi_k\}_{-1}^N$ follows a recurrence formula which is

$$\begin{cases} \pi_{k+1} = (I - a_k)\pi_k - b_k\pi_{k-1} & \text{(a)} \\ \pi_{-1} = 0 & \text{(b)} \\ \pi_0 = 1 & \text{(c)} \end{cases} \tag{39}$$

This recurrence formula is equivalent to

$$I\tilde{\pi} = \begin{pmatrix} a_0 & 1 & & \\ b_1 & a_1 & 1 & \\ & \ddots & \ddots & \ddots \\ & & b_{N-1} & a_{N-1} \end{pmatrix}\tilde{\pi} + \begin{pmatrix} 0 \\ \vdots \\ 0 \\ \pi_N(I) \end{pmatrix} \tag{40}$$

with

$$\tilde{\pi} = \begin{pmatrix} \pi_0(I) \\ \pi_1(I) \\ \vdots \\ \pi_{N-1}(I) \end{pmatrix} \tag{41}$$

The tridiagonal matrix in the right-hand side of Eq. (40) is similar to a *Jacobi* matrix (Gautschi, 2004; Press and Teukolsky, 1990):

$$J_N = \begin{pmatrix} a_0 & \sqrt{b_1} & & \\ \sqrt{b_1} & a_1 & \sqrt{b_2} & \\ & \ddots & \ddots & \ddots \\ & & \sqrt{b_{N-1}} & a_{N-1} \end{pmatrix} \tag{42}$$

Then, as the nodes $\{\widehat{I}_l^k\}_1^N$ are the roots of π_N, they are also the eigenvalues of J_N (see Eq. (40)). Conventional numerical methods can be used to obtain eigenvalues from the matrix coefficients a_k and b_k (Press and Teukolsky, 1990). The key point of the QMoM algorithm is to compute the coefficients $\{a_k\}_0^{N-1}$ and $\{b_k\}_1^{N-1}$ from the moments $\{m_l^\alpha\}_0^{2N-1}$ with an efficient method. The *Product-Difference algorithm* developed by Gordon is an effective way used here to perform this computation (Gordon, 1968; McGraw, 1997).

The nodes are therefore obtained from the eigenvalues of the *Jacobi* matrix. Concerning the weights, they can be also computed from the *Jacobi* matrix eigenvectors. Indeed, if $u_{k,1}$ is the first component of the kth normalized eigenvector of J_N, the expression used in literature for calculating the kth weight is (Gautschi, 2004; Press and Teukolsky, 1990)

$$\hat{x}_l^k = m_{l,0}u_{k,1}^2 \tag{43}$$

3. Results analysis

3.1. Test case description

The example studied in this part considers kerosene droplets vaporizing in air rich in vapor. The vapor is composed with the most volatile component of the kerosene. This test case has been chosen since it is relevant for the investigation of QMoM application to the multi-component droplet vaporization modeling. Indeed, the vapor condensation phenomenon was not properly solved by the Gamma-PDF model since, in this case, the droplet composition PDF does not fit with a Γ function (Harstadt et al., 2003). It is then appealing to test QMoM for a condensation test case. This example is also fulfilling to study other significant points of interest, such as the *Continuous Thermodynamic* hypotheses and the QMoM convergence. The reference model used to perform this study is the *Discrete Component Model* (DCM) which solves droplet composition equations for each component of the mixture.

The test case presented in this paper studies the evaporation of kerosene droplets vaporizing in air mixed with vapor of iso-C_6H_{14}, the most volatile component of kerosene ($T_{nb}^{iso-C_6H_{14}} = 331$ K). The droplets are 50 μm diameter and their initial temperature is 300 K. The surrounding gas temperature and the ambient pressure are supposed to remain constant. They are fixed respectively to $500K$ and $5bar$. The initial composition of the carrier gas is $x_{g,\infty}^{air} = 0.7$ and $x_{g,\infty}^{iso-C_6H_{14}} = 0.3$. The vapor composition evolution is computed from a two-way coupling approach applied to the mass conservation equation of each component. The droplet's concentration is equal to 10^{11} droplets m^{-3}. Kerosene droplets are studied and their initial composition is plotted according to the different model. For the *Discrete Component Model* (DCM), the mole fractions of each component of the kerosene are plotted in Fig. 2. Then, the PDF corresponding to the Γ-*Continuous Thermodynamic Model* (Γ-CTM) is displayed in Fig. 3 and finally, the nodes and the weights of the quadrature method of moments (QMoM) are represented in Fig. 4. The corresponding moments for the kerosene composition are given in Table 1.

3.2. Global evolutions

Droplet vaporization has been computed using different methods for modeling the droplet composition. The *Discrete Component Model* (DCM) provides the reference solution which is compared to the other *Continuous Thermodynamic* methods, the Γ-CTM and the QMoM. The droplet's vapor flow rate is first analyzed to understand the vaporization phenomenon. Following Fig. 5, vapor first condenses (i.e., the vapor flow rate is negative) and then, when the droplet is rich enough in iso-C_6H_{14}, it evaporates (i.e., the vapor flow rate is positive). In comparison to the Γ-CTM approach, the QMoM results are closer to the reference model (DCM) and, as expected, this is improved by increasing the number of

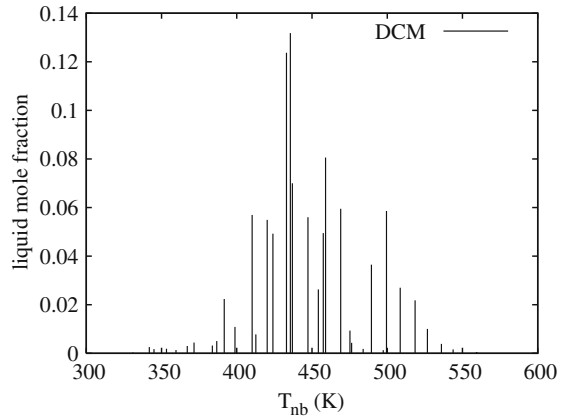

Fig. 2. Composition of the kerosene used in the *Discrete Component Model* (36 components).

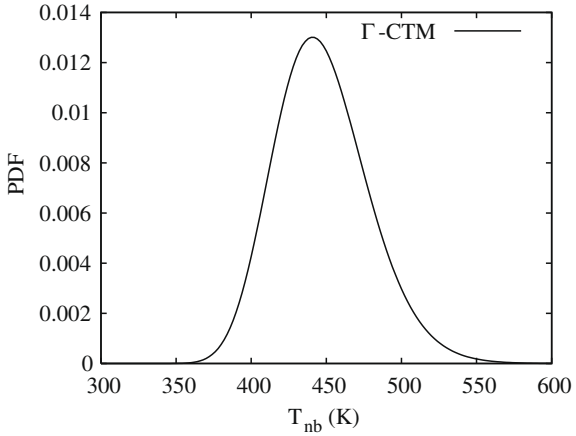

Fig. 3. PDF of the kerosene for the Γ-*Continuous Thermodynamic Model*.

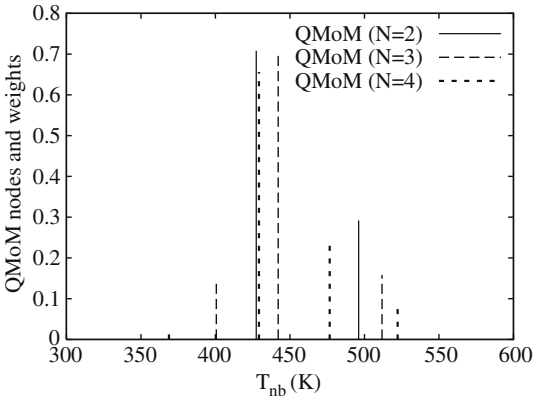

Fig. 4. Nodes and weights of the kerosene for the quadrature method of moments ($N = 2, N = 3$ and $N = 4$).

pseudo-components (i.e., $N = 3$ instead of $N = 2$). The inaccuracy of the Γ-CTM approach for the vapor flow rate computation is truly due to a large discrepancy of this model concerning the droplet composition modeling. This can be noticed from the first order moment evolution (see Fig. 6). After the vapor condensation, the droplet composition PDF is not anymore mono-modal and consequently the Γ-CTM fails whereas the QMoM computes a

Table 1
Moments of the kerosene composition.

Moment order (α)	Moment for the droplet composition (m_l^α)
0	$1.0000000000 \times 10^{0}$
1	$4.4745608709 \times 10^{2}$
2	$2.0119347196 \times 10^{5}$
3	$9.0927061540 \times 10^{7}$
4	$4.1313264695 \times 10^{10}$
5	$1.8875531070 \times 10^{13}$
6	$8.6738050766 \times 10^{15}$
7	$4.0095554609 \times 10^{18}$

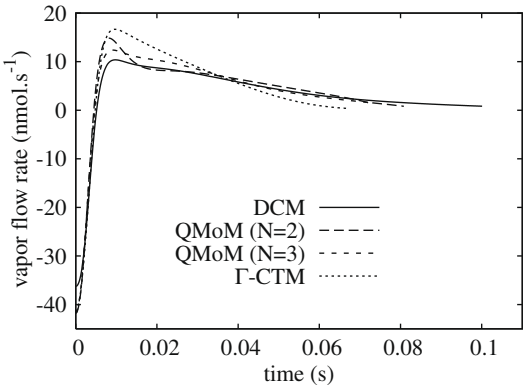

Fig. 5. Comparisons between models for the vapor flow rate.

satisfactory solution. The analysis of QMoM results is completed with the study of node and weight evolutions.

3.3. Node and weight evolutions

The QMoM nodes and weights are displayed for the droplet's and the vapor's compositions. The results are provided for QMoM $N = 3$ (i.e, with three pseudo-components). The iso-C_6H_{14} condensation is noticeable from the increasing of iso-C_6H_{14} mole fraction in the droplet's composition (see weight 1 in Fig. 7) and from its decreasing in the vapor's composition (see weight 1 on Fig. 8). The vaporization phenomenon is then characterized by an accumulation of heavy components in the droplet (see weight 3 in Fig. 7). The analysis of node variations shows that the nodes quickly plateau (see Figs. 9 and 10). Once the nodes are such as $\widehat{l}_l^k(t + \Delta t) = \widehat{l}_l^k(t)$, they remain constant since an obvious solution of Eq. (27) using QMoM moment expressions Eq. (3) is actually $\widehat{l}_l^k(t + \Delta t) = \widehat{l}_l^k(t)$ and

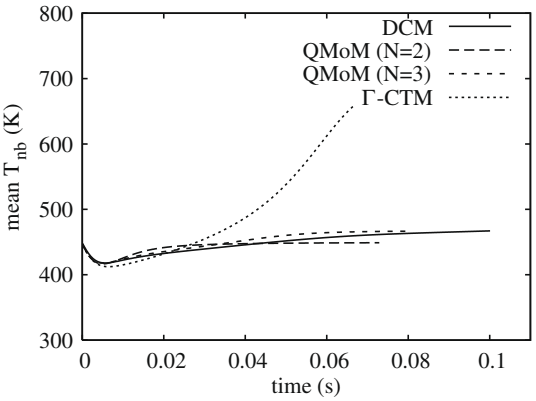

Fig. 6. Comparisons between models for the first order moment (mean T_{nb}).

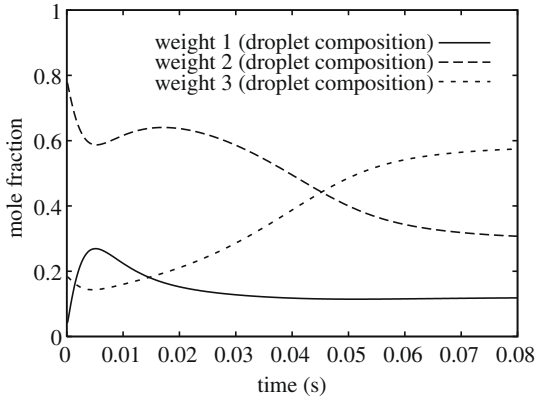

Fig. 7. Evolution of the QMoM weights for the droplet composition.

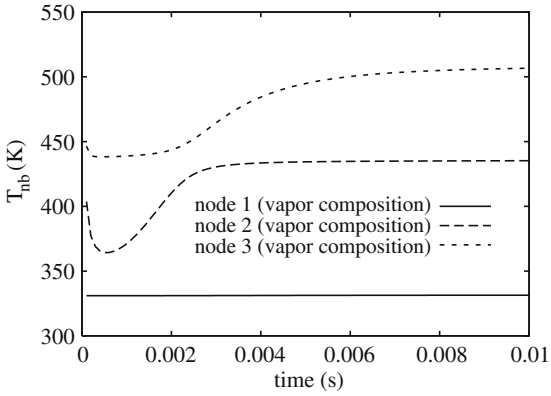

Fig. 10. Evolution of the QMoM nodes for the vapor composition.

$$\hat{x}_l^k(t+\Delta t) = \left(1+\frac{3\dot{n}^{tot}}{4\pi R^3 c_l}\Delta t\right)\hat{x}_l^k(t) - \frac{3\Delta t}{4\pi R^3 c_l}\frac{\dot{n}^{tot}(1+B_M)}{B_M} \times \frac{P_{sat}(\widehat{T}^k)}{P_\infty}\hat{x}_l^k(t) + \frac{3\Delta t}{4\pi R^3 c_l}\frac{\dot{n}^{tot}}{B_M}\hat{x}_{g,\infty}^k(t) \quad (44)$$

Therefore, in this simplified test case which considers only the vaporization phenomenon, the nodes quickly converge and then, the weight evolution is the same as in a *Discrete Component Model*.

3.4. Convergence

The outcomes of the *Continuous Thermodynamic* hypotheses have to be studied in order to point out the best solution which can be obtained using a CTM approach. The CTM methods (Gamma-PDF model, QMoM) tend toward this solution which corresponds to the solution provided by the DCM model using the CTM hypotheses. The two main *Continuous Thermodynamic* hypotheses are the interpolation of the physical properties as functions of I (see **Hypothesis 1**) and the same diffusion coefficient and *Sherwood* number for all components (see **Hypothesis 2**). This last hypothesis is equivalent to assume the same *Spalding* number B_M for all components (see Eq. (13)).

The vapor condensation test case has been computed with the *Discrete Component Model*. The two CTM hypotheses have been successively added to analyze the effects of both of them (see Fig. 11). The results obtained show that the **Hypothesis 2** is the most significant source of error. Indeed, the vapor is mainly composed with a volatile component, the iso-C_6H_{14}, and consequently the value of the *Spalding* number is characteristic of a volatile component. This explained why the droplet lifetime is underestimated when *Continuous Thermodynamic* approaches are used in this case: there is an early vaporization of "heavy" components, and consequently a shortening of the droplet vaporization time. The CTM results remain quite satisfying for all that, since the mass of the droplet at the end of the vaporization is almost insignificant to alter CFD computations. The optimal CTM solution has been thus analyzed and serves as the reference solution to study QMoM convergence.

The number of pseudo-components used in the QMoM approach has been increased up to $N = 4$ in order to study the QMoM convergence. The results are displayed in Fig. 12. They point out the improvement of the accuracy with the number of pseudo-components since the composition is then better modeled, and they

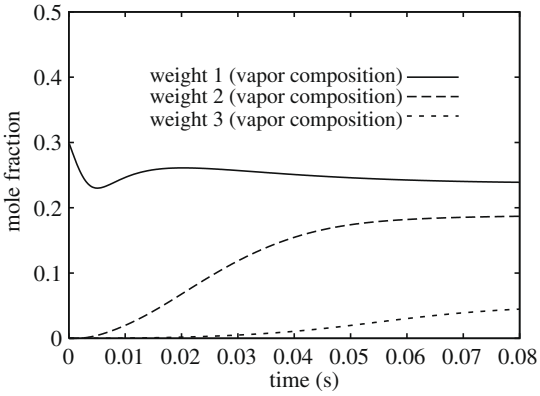

Fig. 8. Evolution of the QMoM weights for the vapor composition.

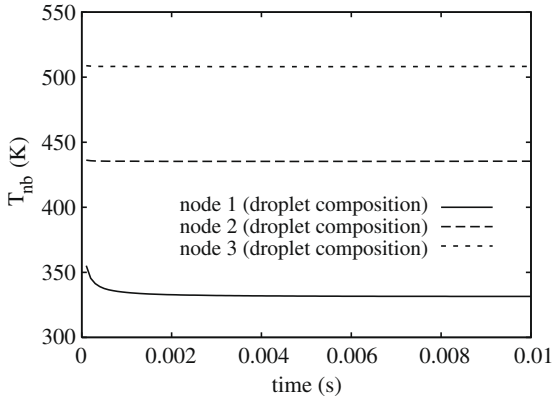

Fig. 9. Evolution of the QMoM nodes for the droplet composition.

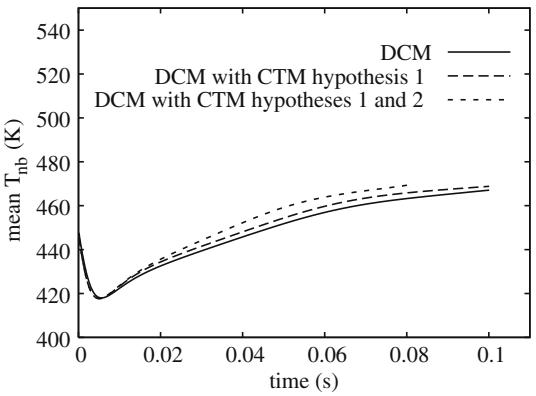

Fig. 11. CTM error analysis for the first order moment (mean T_{nb}).

show that the convergence is reached for three pseudo-components. Indeed, the QMoM results for $N = 3$ are very close to the optimal CTM solution (i.e., DCM solution with CTM hypotheses) and it is worth noticing that there is no real improvement for $N = 4$ (i.e., with four pseudo-components). This observation made in this case has been actually experienced and confirmed for various examples. The QMoM appears therefore to be quite suitable to solve the CTM approach of the multi-component droplet vaporization modeling since only three pseudo-components are required to obtain the convergence. Consequently, the accuracy can be combined with efficient computations.

3.5. Computational efficiency

The various methods have been tested to analyze their computational cost (see Table 2). The QMoM approach appears slightly more time-consuming than the Γ-CTM model, due to the algorithm used in QMoM for finding the *Jacobi* matrix eigenvalues. However, the *Moment Problem* can be analytically solved using two pseudo-components ($N = 2$). The QMoM has then the same computation time as the Γ-CTM and this can be an advantageous solution for computations with strong time constraints.

4. Concluding remarks

In this article, the quadrature method of moments (QMoM) has been applied for solving the *Continuous Thermodynamic Model* of multi-component droplet vaporization. According Lage who has implemented this method for vapor–liquid equilibrium (Lage, 2007), this article extends the QMoM scope to the modeling of the droplet vaporization phenomenon. The aim of this research work is actually to provide a numerical method which allows to implement a multi-component vaporization model in CFD codes. The accuracy, the robustness and the low computational cost are therefore three significant requirements which have been analyzed in this study.

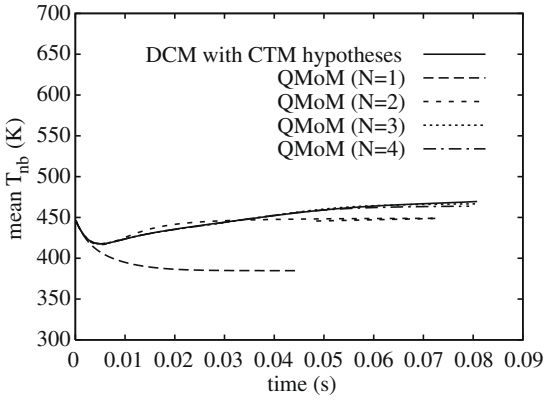

Fig. 12. Convergence study for the first order moment (mean T_{nb}).

Table 2
Computation times of the different models.

Model	CPU time
DCM (36 components)	100
T-CTM	4
QMoM $N = 2$ (analytic solution)	4
QMoM $N = 2$ (numerical solution)	6
QMoM $N = 3$ (numerical solution)	7.5

Consequently, a particular importance has been attached to the understanding of the QMoM mathematical background. Indeed, the results coming from the *Moment Problem* theory have permitted to demonstrate the QMoM robustness. The existence of a solution to the QMoM modeling has been proved under an explicit condition about the time step. This point is relevant for the implementation of such a method in industrial CFD codes, since robustness is critical for complex applications.

Then, the QMoM has been tested in the difficult case of the vapor condensation. The results have pointed out a clear improvement using the QMoM rather than the Gamma-PDF model. More over, the convergence study has shown that the optimal CTM solution is reached with only three pseudo-components ($N = 3$). The QMoM computation is a little bit more time-consuming for $N \geqslant 3$ than the Gamma-PDF model. However, the same computation time can be obtained using two pseudo-components (i.e., using the analytic solution). In this case, the results remain quite satisfactory, even if the convergence is not reached.

Consequently, the various properties of the QMoM which have been demonstrated in this article, give convincing arguments for the implementation of this method in CFD codes. The QMoM is then promising for computing multi-component droplet vaporization in case of industrial applications.

Acknowledgments

The authors are grateful to the ASTRA program founded by CNRS and ONERA. This program concerns the study of multi-component sprays.

Appendix A. Physical properties in *Continuous Thermodynamics*

The physical properties given in this section are obtained following the procedure detailed in Section 2.2 which describes the conversion from the physical properties of real components used in *Discrete Component Model* (DCM) to the physical properties of pseudo-components used in *Continuous Thermodynamic Models* (CTM). The relationships used for the DCM physical properties to get then CTM interpolations are taken from Reid's book (Reid et al., 1977). The values given afterwards for the various coefficients are those obtained and implemented for the kerosene composition studied in this paper.

Molar mass (kg kmol^{-1}):

$$M(I) = A_0 + A_1 I \tag{A.1}$$

$A_0 = -123.60$ and $A_1 = 0.6247$.

Critical temperature (K):

$$T_c(I) = A_0 + A_1 I \tag{A.2}$$

$A_0 = 205.95$ and $A_1 = 0.9046$.

Latent heat of vaporization (J kmol^{-1}):

$$l_v(I) = (A_0 + A_1 I)\left(\frac{T_c(I) - T_S}{T_c(I) - I}\right)^{0.38} \tag{A.3}$$

$A_0 = -3.7607.10^6$ and $A_1 = 9.4865.10^4$.

Saturation vapor pressure (Pa):
Clausius-Clapeyron expression:

$$P_{sat}(I) = P_0 exp\left[\frac{(A_0 + A_1 I)}{\Re}\left(\frac{1}{I} - \frac{1}{T_S}\right)\right] \tag{A.4}$$

$A_0 = -3.7607.10^6$ and $A_1 = 9.4865.10^4$.

Vapor heat capacity (J kmol^{-1} K^{-1}):

$$Cp_g(I) = (A_0 + A_1 I) + (B_0 + B_1 I)T_g + (C_0 + C_1 I)T_g^2 \quad (A.5)$$

$A_0 = 1.7478.10^4, A_1 = -1.0038.10^1, B_0 = -8.0648.10^2, B_1 = 3.8658,$
$C_0 = 3.5307.10^{-1}, C_1 = -1.5673.10^{-3}.$

Vapor viscosity (kg m^{-1} s^{-1}):

$$\mu_g(I) = (A_0 + A_1 I) + (B_0 + B_1 I)T_g \quad (A.6)$$

$A_0 = 3.2941.10^{-6}, A_1 = -4.5702.10^{-9}, B_0 = 2.4177.10^{-8}, B_1 = -1.9742.10^{-11}.$

Vapor thermal conductivity (J m^{-1} K^{-1} s^{-1}):

$$\lambda_g(I) = (A_0 + A_1 I) + (B_0 + B_1 I)T_g + (C_0 + C_1 I)T_g^2 \quad (A.7)$$

$A_0 = -6.8725.10^{-3}, A_1 = 9.8134.10^{-6}, B_0 = 3.5028.10^{-5},$
$B_1 = -6.4010.10^{-8}, C_0 = 2.263.10^{-7}, C_1 = -2.5570.10^{-10}.$

Vapor diffusion coefficient (m^2 s^{-1}):

The following relationship for D_g is function of the ambient pressure P expressed in *atm*, the ambient temperature T_g in *K*, the molar mass expressed in $g.mol^{-1}$ and the molecular diffusion volume v.

$$D_g(I) = \frac{10^{-7} T_g^{1.75} \left[\frac{M(I)+M^{air}}{M(I)M^{air}(I)}\right]^{\frac{1}{2}}}{P\left[(v_{g,0} + v_{g,1} I)^{\frac{1}{3}} + v_g^{air\frac{1}{3}}\right]^2} \quad (A.8)$$

$v_{g,0} = -1.7926.10^2, \; v_{g,1} = 9.113.10^{-1}.$

Liquid molar volume density (kmol m^{-3}):

$$c_l(I) = \left(A_0 + A_1 I + A_2 I^2\right) + \left(B_0 + B_1 I + B_2 I^2\right) T_l \quad (A.9)$$

$A_0 = 4.2163.10^1, A_1 = -1.3445.10^{-1}, A_2 = 1.2442.10^{-4},$
$B_0 = -7.1106.10^{-2}, B_1 = 2.5921.10^{-4}, B_2 = -2.5284.10^{-7}.$

Liquid heat capacity (J kmol^{-1} K^{-1}):

$$Cp_l(I) = (A_0 + A_1 I) + (B_0 + B_1 I)T_l \quad (A.10)$$

$A_0 = -2.2873.10^5, A_1 = 8.2549.10^2, B_0 = -7.8088.10^1, B_1 = 1.6086.$

Liquid viscosity (kg m^{-1} s^{-1}):

$$log(\mu_l(I)) = \left(A_0 + A_1 I + A_2 I^2\right)\left(\frac{1}{T_l} - \frac{1}{\left(B_0 + B_1 I + B_2 I^2\right)}\right) - 3 \quad (A.11)$$

$A_0 = -5.8043.10^2, A_1 = 4.1835, A_2 = -3.568.10^{-3},$
$B_0 = -1.7951.10^2, B_1 = 1.6782, B_2 = -1.4098.10^{-3}.$

Liquid thermal conductivity (J m^{-1} K^{-1} s^{-1}):

$$\lambda_l(I) = (A_0 + A_1 I) + (B_0 + B_1 I)T_l + (C_0 + C_1 I)T_l^2 \quad (A.12)$$

$A_0 = 5.355.10^{-2}, A_1 = 5.0987.10^{-4}, B_0 = -2.5251.10^{-4},$
$B_1 = -7.9625.10^{-7}, C_0 = 2.483.10^{-7}, C_1 = 3.2996.10^{-10}.$

References

Arias-Zugasti, M., Rosner, D.E., 2003. Multi-component fuel droplet vaporization and combustion using spectral continuous mixture theory. Combust. Flame 135, 271–284.

Cotterman, R.L., Bender, R., Prausnitz, J.M., 1985. Phase equilibria for mixtures containing very many components. Development and applications of continuous thermodynamics for chemical process design. Ind. Eng. Chem. Process Des. Dev. 24, 194–203.

Curto, R.E., Fialkow, L.A., 1991. Recursiveness, positivity, and truncated moment problems. Houston J. Math. 17, 603–635.

Desjardins, O., Fox, R.O., Villedieu, P., 2008. A quadrature-based moment method for dilute fluid-particle flows. J. Comp. Phys. 227, 2514–2539.

Gautschi, W., 2004. Orthogonal Polynomial – Computation and Approximation. Oxford University Press.

Gordon, R.G., 1968. Error bounds in equilibrium statistical mechanics. J. Math. Phys. 9, 655–663.

Hallett, W.L.H., 2000. A simple model for the vaporization of droplets with large numbers of components. Combust. Flame 121, 334–344.

Harstadt, K.G., Le Clercq, P., Bellan, J., 2003. Statistical model of multicomponent-fuel drop evaporation for many-droplet liquid–gas flow simulations. AIAA J. 41, 1858–1874.

Lage, P.L.C., 2007. The quadrature method of moments for continuous thermodynamics. Comput. Chem. Eng. 31, 782–799.

Laurent, C., Lavergne, G., Villedieu, P., 2009. Continuous thermodynamics for droplet vaporization: comparison between Gamma-PDF model and QMoM. C.R. Mecanique 337, 449–457.

Marchisio, D.L., Fox, R.O., 2005. Solution of population balance equations using the direct quadrature method of moments. J. Aerosol Sci. 36, 43–73.

McGraw, R., 1997. Description of aerosol dynamics by the quadrature method of moments. Aerosol Sci. Technol. 27, 255–265.

Press, W.H., Teukolsky, S.A., 1990. Orthogonal polynomials and gaussian quadrature with nonclassical weight. Comput. Phys. 4, 423–426.

Reid, R.C., Prausnitz, J.M., Sherwood, T.K., 1977. The Properties of Gases and Liquids, Third ed. McGraw-Hill, New York.

Shohat, J.A., Tamarkin, J.D., 1943. The Problem of Moments. Am. Math. Soc., New York.

Sirignano, W.A., 1999. Fluid Dynamics and Transport of Droplets and Sprays. Cambridge University Press.